Cell, Vol. 107, 323–337, November 2, 2001, Copyright ©2001 by Cell Press

Loss of the *Suv39h* Histone Methyltransferases Impairs Mammalian Heterochromatin and Genome Stability

Antoine H.F.M. Peters,[1,5] Dónal O'Carroll,[1,5,6] Harry Scherthan,[2,6] Karl Mechtler,[1] Stephan Sauer,[1] Christian Schöfer,[3] Klara Weipoltshammer,[3] Michaela Pagani,[1] Monika Lachner,[1] Alexander Kohlmaier,[1] Susanne Opravil,[1] Michael Doyle,[1,6] Maria Sibilia,[1,6] and Thomas Jenuwein[1,4]

[1] Research Institute of Molecular Pathology (IMP)
Vienna Biocenter
Dr. Bohrgasse 7
A-1030 Vienna
Austria

[2] Department of Human Biology
University of Kaiserslautern
Erwin-Schrödingerstrasse, Geb. 14
D-67663 Kaiserslautern
Germany

[3] Institute of Histology and Embryology
University of Vienna
Schwarzspanierstraße 17
A-1090 Vienna
Austria

Summary

Histone H3 lysine 9 methylation has been proposed to provide a major "switch" for the functional organization of chromosomal subdomains. Here, we show that the murine Suv39h histone methyltransferases (HMTases) govern H3-K9 methylation at pericentric heterochromatin and induce a specialized histone methylation pattern that differs from the broad H3-K9 methylation present at other chromosomal regions. *Suv39h*-deficient mice display severely impaired viability and chromosomal instabilities that are associated with an increased tumor risk and perturbed chromosome interactions during male meiosis. These in vivo data assign a crucial role for pericentric H3-K9 methylation in protecting genome stability, and define the *Suv39h* HMTases as important epigenetic regulators for mammalian development.

Introduction

Chromatin represents the physiological template of the genetic information in all eukaryotic cells, and is functionally divided into euchromatic and heterochromatic regions. This functional distinction has been proposed to be crucial for epigenetic control of gene expression programs (Turner, 2000; Jenuwein and Allis, 2001), to underlie the specialized chromatin structure surrounding centromeres and telomeres (Karpen and Allshire, 1997) and to facilitate the extensive reorganization of chromosomes during meiosis (Karpen et al., 1996; Dernburg et al., 1996). Although alterations in chromatin structure can be induced by sequence-specific recruitment of transcription factors and chromatin remodeling complexes (Kingston and Narlikar, 1999), or by the clustering of DNA repeats (Csink and Henikoff, 1998), DNA sequence per se appears not to be sufficient to mediate the establishment of distinct chromosomal subdomains (Murphy and Karpen, 1998; Henikoff et al., 2001). Further, while changes in DNA methylation patterns correlate with distinct epigenetic states (Bird and Wolffe, 1999), DNA methylation is virtually absent in *S. pombe* and rare in *Drosophila* (Lyko, 2001), despite the epigenetic control operating in these organisms.

Recently, a "histone code" hypothesis has been suggested (Strahl and Allis, 2000), which predicts that different modifications (e.g., acetylation, phosphorylation, methylation) of histone N termini are interdependent and represent an evolutionarily conserved mechanism that can induce and stabilize functionally distinct chromosomal subdomains (Jenuwein and Allis, 2001). For example, general underacetylation of histones (Jeppesen et al., 1992; Ekwall et al., 1997) and phosphorylation of histone H3 (Hendzel et al., 1997; Wei et al., 1999) are required for faithful chromosome segregation, presumably by preserving the more compacted chromatin structure of pericentric heterochromatin. Furthermore, the discovery of mammalian histone H3 lysine 9 specific histone methyltransferases (Suv39h HMTases) (Rea et al., 2000), which are heterochromatin-enriched enzymes transiently accumulating around centromeres during mitosis (Aagaard et al., 2000), revealed a regulatory mechanism in which the selective methylation of histone H3 at lysine 9 (H3-K9) creates a high-affinity binding site for the heterochromatic HP1 proteins (Lachner et al., 2001; Bannister et al., 2001; Nakayama et al., 2001). Gain- and loss-of-function studies for Suv39h enzymes in mammalian cell lines (Melcher et al., 2000; Rea et al., 2000) suggest a major role for the SUV39H1-HP1 methylation system in chromosome segregation. In addition, the SUV39H1 HMTase is also involved in local gene repression (Firestein et al., 2000), and is targeted to specific cell cycle genes through the tumor suppressor Rb (Nielsen et al., 2001).

In *S. pombe*, the *clr4* and *swi6* genes, which encode the fission yeast homologs of SUV39H1 and HP1, are required for heterochromatic gene silencing (Thon et al., 1994; Allshire et al., 1995; Ivanova et al., 1998) and centromere function (Ekwall et al., 1996). Disruption of the HMTase activity of Clr4 prevents pericentric association of Swi6 protein (Bannister et al., 2001) and impairs H3-K9 methylation (Nakayama et al., 2001). Although *clr4* and *swi6* null mutants are viable, mutation of either locus leads to high rates of chromosome missegregation (Ekwall et al., 1996). By contrast, *HP1* null mutants are lethal in *Drosophila* (Eissenberg et al., 1992) and display a more severe phenotype, including aberrant chromosome segregation and telomeric fusions (Kellum

[4] Correspondence: jenuwein@nt.imp.univie.ac.at

[5] These authors contributed equally to this work

[6] Present addresses: (D.O'C.) The Rockefeller University, New York; (H.S.) Max Planck Institute for Molecular Genetics, Berlin; (M.D.) Institute of Botany, Vienna University; (M.S.) Institute of Dermatology, Vienna University

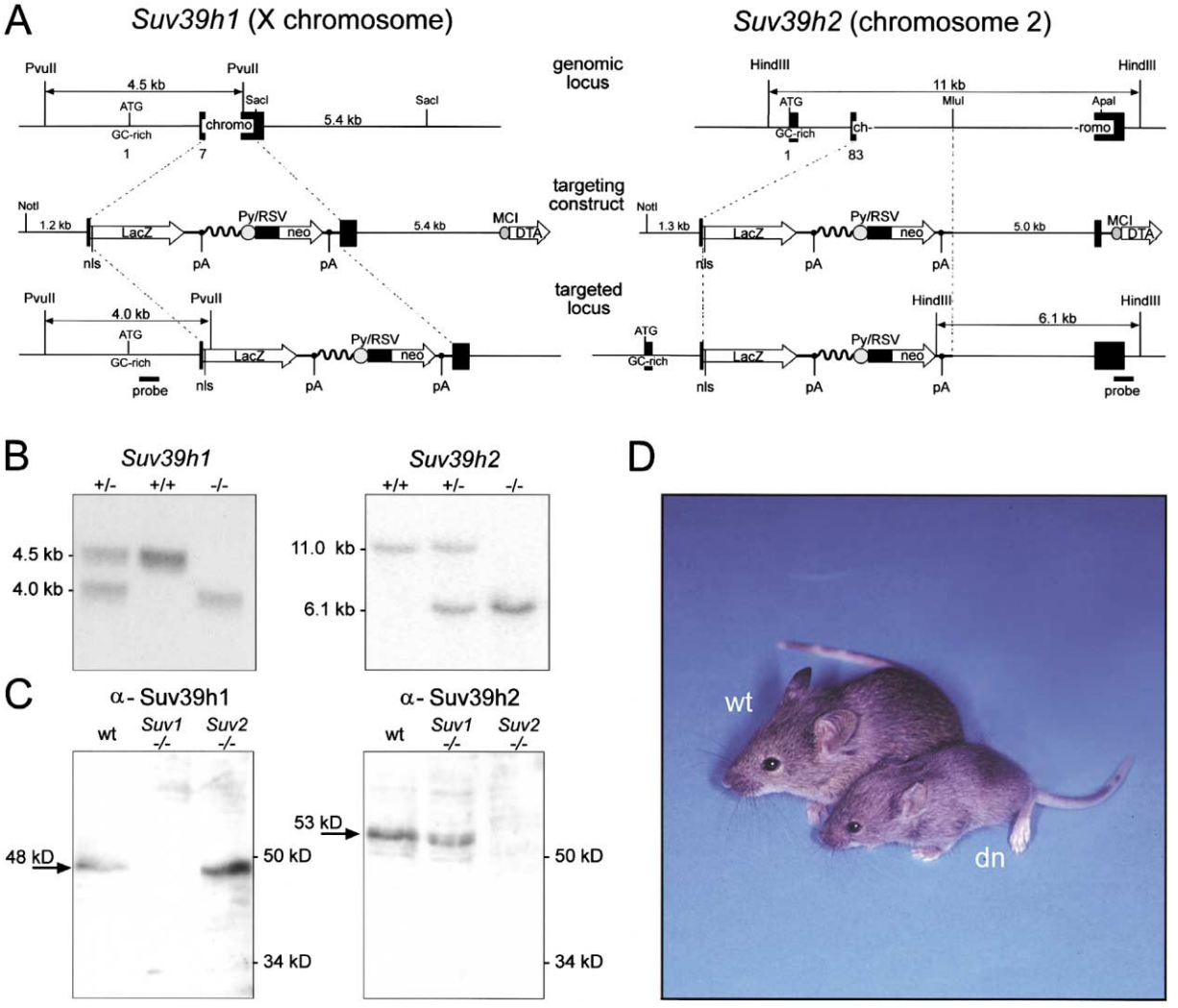

Figure 1. Targeting and Genotyping of *Suv39h1*- and *Suv39h2*-Deficient Mice

(A) Diagrammatic representation of the *Suv39h1* and *Suv39h2* genomic loci, the replacement vectors and the targeted alleles. Exons are indicated by black boxes with numbers referring to the starting amino acid positions of the respective exons (O'Carroll et al., 2000). Also shown are the diagnostic restriction sites and the external probes used for Southern blot analyses.

(B) Southern blot analyses of PvuII- or HindIII-digested DNA isolated from offspring of *Suv39h1*+/− or *Suv39h2*+/− intercrosses.

(C) Protein blot analyses of testis nuclear extracts from wild-type (wt), *Suv39h1*−/− (*Suv1*−/−), and *Suv39h2*−/− (*Suv2*−/−) mice with α-Suv39h1 and α-Suv39h2 antibodies.

(D) *Suv39h* double null (dn) mice are growth retarded at birth and during adulthood.

and Alberts, 1995; Fanti et al., 1998). Surprisingly, *Su(var)3-9* mutants (Tschiersch et al., 1994) have so far not revealed chromosome segregation defects in *Drosophila*.

A genetic analysis of mammalian heterochromatin and its role in epigenetic gene control and chromosome stability has been lacking. The murine Suv39h HMTases are encoded by two loci, *Suv39h1* and *Suv39h2*, which show overlapping expression profiles during embryogenesis, while in adult mice *Suv39h2* is mainly expressed in testes (O'Carroll et al., 2000). These data suggest redundant roles for the Suv39h HMTases during embryonic development and a putative additional function in the male germline. To address the functional consequence(s) of Suv39h-dependent H3-K9 methylation during mammalian development, we disrupted the *Suv39h1* and *Suv39h2* gene loci in the mouse. In addition, we developed α-methH3-K9 antibodies which selectively recognize H3-K9 methylation in heterochromatic subdomains.

Here, we demonstrate that the Suv39h HMTases regulate H3-K9 methylation at pericentric heterochromatin. Combined disruption of both *Suv39h* HMTase genes severely impairs viability and induces chromosomal instabilities plus an increased risk of tumorigenesis. In addition, *Suv39h* double null male mice display complete spermatogenic failure that is largely caused by nonhomologous chromosome associations. Together, these in vivo results assign a direct role for Suv39h-dependent H3-K9 methylation at pericentric heterochromatin in protecting genome stability during mammalian development.

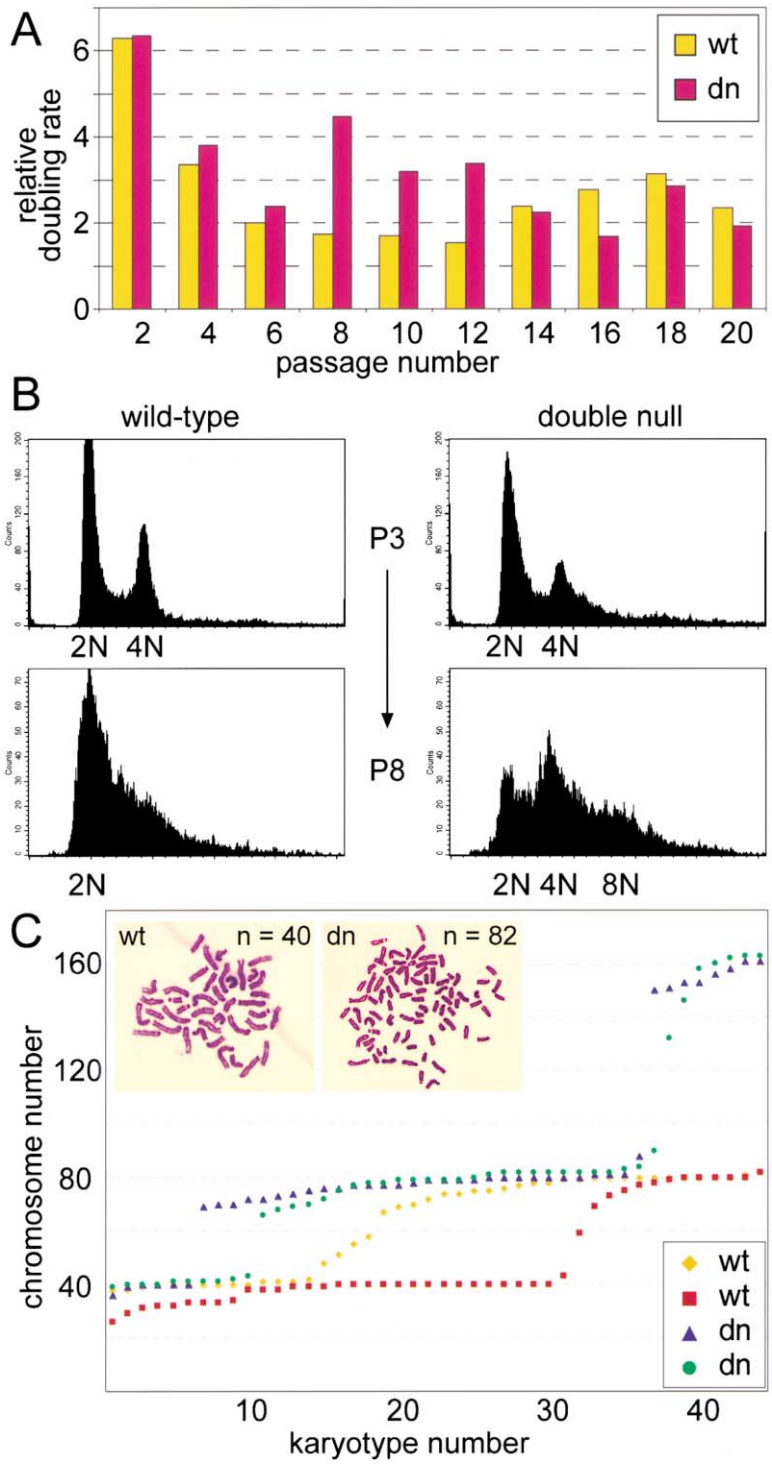

Figure 2. Chromosomal Instabilities in *Suv39h* dn PMEFs

(A) Relative doubling rates of wild-type (wt) and *Suv39h* dn (double null) PMEFs determined in a 3T3 protocol over the first 20 passages.

(B) DNA contents of wt and *Suv39h* dn PMEF mass cultures at passage 3 and passage 8.

(C) Statistical karyotype analysis with two wt and two *Suv39h* dn PMEF cultures at passage 8. For each culture, 45 metaphases were evaluated. Insets display metaphase spreads showing a diploid number (n = 40) of chromosomes for wt and a hyper-tretraploid number (n = 82) of chromosomes for *Suv39h* dn PMEFs.

Results

Targeted Disruption of the *Suv39h1* and *Suv39h2* Gene Loci in the Mouse Germline

Murine Suv39h HMTases are encoded by two loci which have been mapped to centromere-proximal positions in the X chromosome (*Suv39h1*) or in chromosome 2 (*Suv39h2*) (O'Carroll et al., 2000). Both gene loci were independently disrupted by homologous recombination in embryonic stem (ES) cells using a conventional targeting approach that replaces parts of the evolutionarily conserved chromo domain with the bacterial *LacZ* gene and an *RSV-neomycin* selecion cassette (Figure 1A). These targeting strategies produce in-frame fusion proteins of the first 40 amino acids of Suv39h1 or of the first 113 amino acids of Suv39h2 with lacZ, which maintain β-galactosidase activities (data not shown). Successfully targeted ES cell clones were used to generate chi-

Table 1. Incidence of B Cell Lymphomas in Mice with Reduced *Suv39h* Gene Dosage

Genotype	*Suv39h* Gene dosage	# of Mice with Tumor	Total # of Mice	% of Mice with Tumor
W1W2	3	0	57	0
W1H2, W1N2, H1N2	0–2	1	22	4.6
H1W2, N1W2	2–3	8	26	30.8
H1H2, N1H2	1–2	20	72	27.8
N1N2	0	2	6	33.3

Abbreviations: W1N2: *Suv39h*1+/+; *Suv39h*2−/−; H1H2: *Suv39h*1+/−; *Suv39h*2+/−; N1H2: *Suv39h*1−/−; *Suv39h*2+/−

meric mice that transmitted the mutated *Suv39h1* or *Suv39h2* alleles through the germline (Figure 1B). Protein blot analyses of testis nuclear extracts from wild-type, *Suv39h1*-, and *Suv39h2*-deficient mice with α-Suv39h1 and α-Suv39h2 specific antibodies (O'Carroll et al., 2000) indicated absence of the respective proteins, demonstrating that we had generated null alleles for both genes (Figure 1C).

Severely Impaired Viability of *Suv39h* Double Null Mice

Mice deficient for either *Suv39h1* or *Suv39h2* display normal viability and fertility (data not shown), and do not exhibit apparent phenotypes. Therefore, we intercrossed *Suv39h1*−/− and *Suv39h2*−/− mice to generate compound *Suv39h* mutants that were then used to derive *Suv39h* double null (dn) mice. *Suv39h* dn mice obtained from several different intercrosses are born at only sub-Mendelian ratios, are growth retarded (Figure 1D), and are characterized by hypogonadism in males. For example, from a total of 197 mice, 46 mice would have been expected to be double null, but only 15 *Suv39h* dn mice (∼33%) were born. Analysis of mouse embryogenesis indicated normal development of *Suv39h* dn fetuses until day E12.5, whereas at later stages, *Suv39h* dn fetuses are smaller and display an increased rate of resorptions and prenatal lethality (data not shown). Together, these results demonstrate that the *Suv39h* genes are required for normal viability, and for pre- and postnatal development.

Chromosome Missegregation in *Suv39h* dn Embryonic Fibroblasts

To examine the *Suv39h*-dependent defects in more detail, we derived primary mouse embryonic fibroblasts (PMEFs) from day E12.5 fetuses. Comparative growth curves between wild-type (wt) and *Suv39h* dn PMEFs in a 3T3 protocol over the first 20 passages indicated that *Suv39h* dn PMEFs displayed a higher doubling rate until passage 12 (Figure 2A). At later passages, the *Suv39h* dn PMEFs appear to have a slightly reduced proliferative potential which further declines upon continued cultivation. DNA profiles of passage 3 and passage 8 wt and *Suv39h* dn PMEFs show that wt PMEFs appear genomically stable at passage 3, whereas *Suv39h* dn PMEFs already contain cells with a greater than 4N DNA material (Figure 2B, top panels). At passage 8, wt PMEFs are largely senesced. By contrast, *Suv39h* dn PMEFs continue to proliferate, although many cells display tetraploid and even octaploid DNA contents (Figure 2B, lower panels).

To further characterize these genomic instabilities, we performed karyotype analyses with passage 8 PMEFs. We examined 45 karyotypes each for two independent wt and *Suv39h* dn PMEF cultures. As shown in Figure 2C, a major fraction of the wt karyotypes are nondiploid, with chromosome numbers ranging from 25 to 82. Aneuploidies were significantly increased in *Suv39h* dn karyotypes and comprised chromosome numbers from 38 to 162. Notably, whereas wt PMEFs display a random array of aneuploid karyotypes, *Suv39h* dn PMEFs are largely hypo-tetraploid or hypo-octaploid. Chromosomes in *Suv39h* dn PMEFs appear of normal morphology and we did not observe Robertsonian fusions. We conclude that the absence of *Suv39h* gene function induces genomic instability, primarily by impairing segregation of the entire set of chromosomes.

Development of B Cell Lymphomas in *Suv39h* Mutant Mice

We next analyzed *Suv39h* mutant mice for tumor incidence. Because the majority of *Suv39h* dn mice are nonviable, we examined distinct *Suv39h* genotypes that differ in their gene dosage for either *Suv39h1* or *Suv39h2*. For example, we expected that random X-inactivation of the X-linked *Suv39h1* gene could increase the tumor risk in *Suv39h1*+/− mice, even in the presence of a functional copy of *Suv39h2,* which is significantly downregulated in most adult tissues (O'Carroll et al., 2000). Examination of 99 mice either heterozygous (het) or null for the *Suv39h1* locus indicated an ∼28% penetrance of tumor formation with an onset between 9 and 15 months of age (Table 1). These tumors are B cell lymphomas (Figure 3A) which, according to FACS profiling (see Experimental Procedures), resemble slowly progressing non-Hodgkin lymphomas in humans (Foon and Gale, 1995). The tumor incidence for late onset B cell lymphomas was ∼33% in the few viable *Suv39h* dn mice ($n = 6$). By contrast, *Suv39h2*+/− or *Suv39h2*−/− mice developed B cell lymphomas at only ≤ 5% penetrance ($n = 21$), and we did not observe tumor formation in control wt mice ($n = 57$).

Immunohistochemistry for H3-K9 methylation with a newly developed antibody (α-4x-methH3-K9, see below) on tissue sections from wt mice indicated broad staining in spleen and lymph nodes (Figure 3B, left panel). The staining was somewhat reduced within germinal centers which contain unstimulated centroblasts. Importantly, H3-K9 methylation was lost in *Suv39h* dn sections (data not shown) and was also largely absent in tumor tissues from *Suv39h1*−/−, *Suv39h2*+/− (null1/het2) mice. In these tumor sections, only a few areas of methH3-K9

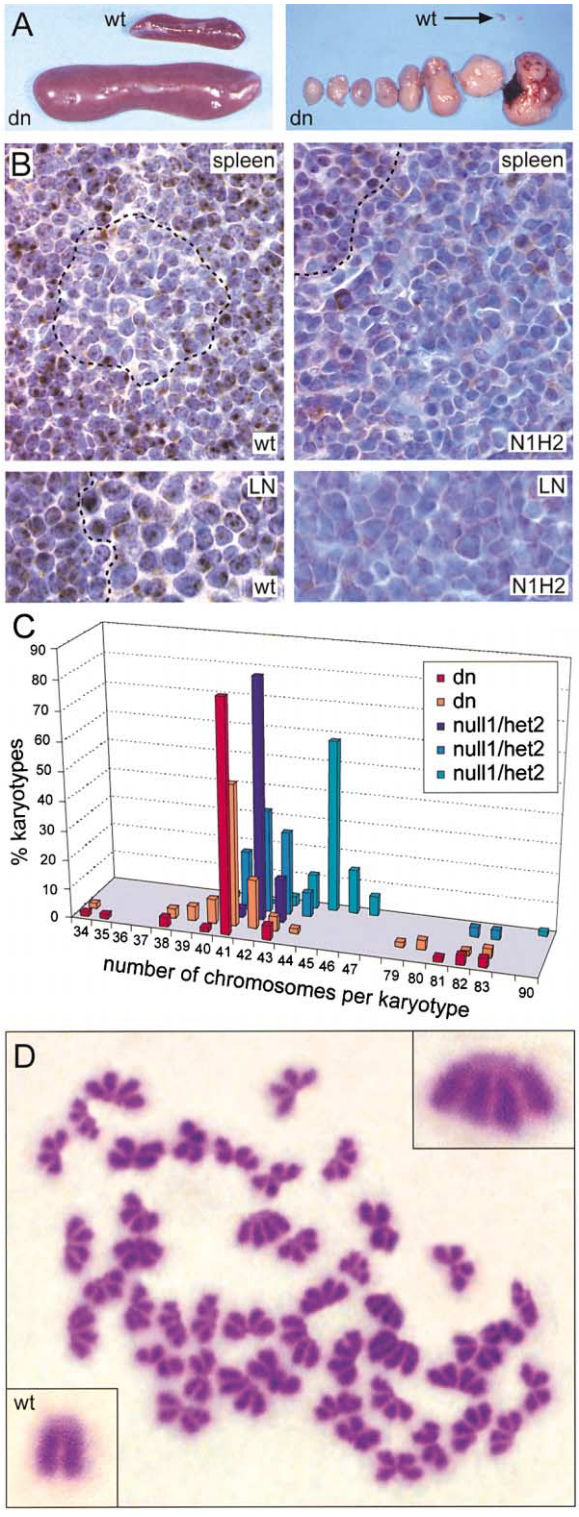

Figure 3. Development of B Cell Lymphomas in *Suv39h* Mutant Mice

(A) Spleen and lymph nodes of an 11-month-old *Suv39h* dn tumor mouse and of a wt control mouse.

(B) Immunohistochemistry with α-4x-methH3-K9 antibodies on tissue sections from wt spleen and lymph nodes (LN) and from *Suv39h* null1/het2 (N1/H2) tumor tissues.

(C) Karyotype analysis of five independent primary cultures derived from the lymph nodes of tumor-bearing *Suv39h* dn and *Suv39h1*−/−, *Suv39h*+/− (null1/het2) mice.

(D) Metaphase spread from a primary B cell lymphoma cell showing "butterfly" chromosomes that remain associated through their acrocentric regions.

positive cells are present which are outgrown by larger B lymphoma cells lacking H3-K9 methylation (Figure 3B, right panel). These results suggest that loss of H3-K9 methylation in null1/het2 and even in null1/wt2 (data not shown) mice can trigger the expansion of tumor cells.

We derived primary cultures from the lymph nodes of *Suv39h* dn and of null1/het2 tumor mice, and analyzed the karyotypes of the B cell lymphoma cells. These tumor cells were largely hyperdiploid but also comprised some hypertetraploid karotypes (Figure 3C). Surprisingly, a fraction of the tumor karyotypes, examined in several independent B cell lymphomas, is characterized by nonsegregated chromosomes that remain attached through their acrocentric regions (Figure 3D). These "butterfly" chromosomes raise the intriguing possibility that the absence of Suv39h HMTase activities could impair the quality and function of pericentric heterochromatin by increasing aberrant interactions between metaphase chromosomes.

Absence of H3-K9 Methylation at *Suv39h* dn Heterochromatin

To assess directly the role of the Suv39h HMTases in histone methylation and heterochromatin organization, we developed a rabbit polyclonal antiserum (α-4x-methH3-K9) that was raised against a "branched" peptide containing four K9-dimethylated H3 N termini (see Experimental Procedures). We reasoned that a more compacted higher-order chromatin conformation might contain an increased density of methylated nucleosomes, thereby presenting multiple H3-K9 dimethylated N termini in close proximity. As shown in Figure 4A, this antiserum indeed detects focal staining in wt PMEFs that significantly overlaps with DAPI-rich heterochromatin. In PMEFs derived from single *Suv39h1*- or *Suv39h2*-deficient mice, ~ 75% of cells still stain positive with these α-4x-methH3-K9 antibodies (data not shown), whereas the staining was abolished in *Suv39h* dn PMEFs (Figure 4A, top panel). Immunoblot analyses with nuclear extracts confirmed a significant reduction of 4x-methH3-K9 signals in *Suv39h* dn PMEFs (Figure 4B, top panel).

We also examined mitotic chromosome spreads from PMEFs (data not shown) and from bone marrow cells with the α-4x-methH3-K9 antiserum. In wt spreads, pericentric heterochromatin was selectively visualized (see insets in Figure 4C), whereas only residual staining was detected in *Suv39h* dn spreads.

Perturbed Patterns of Histone Tail Modifications in *Suv39h* dn Heterochromatin

The above results characterize the α-4x-methH3-K9 antibodies as a cytological marker for heterochromatin. Surprisingly, in comparative analyses with commercially available α-methH3-K9 antibodies that had been raised against a linear peptide presenting only one H3-K9 dimethylated N terminus, we failed to detect selective staining at pericentric heterochromatin in PMEF metaphase chromosomes (Figure 4D) or pronounced enrich-

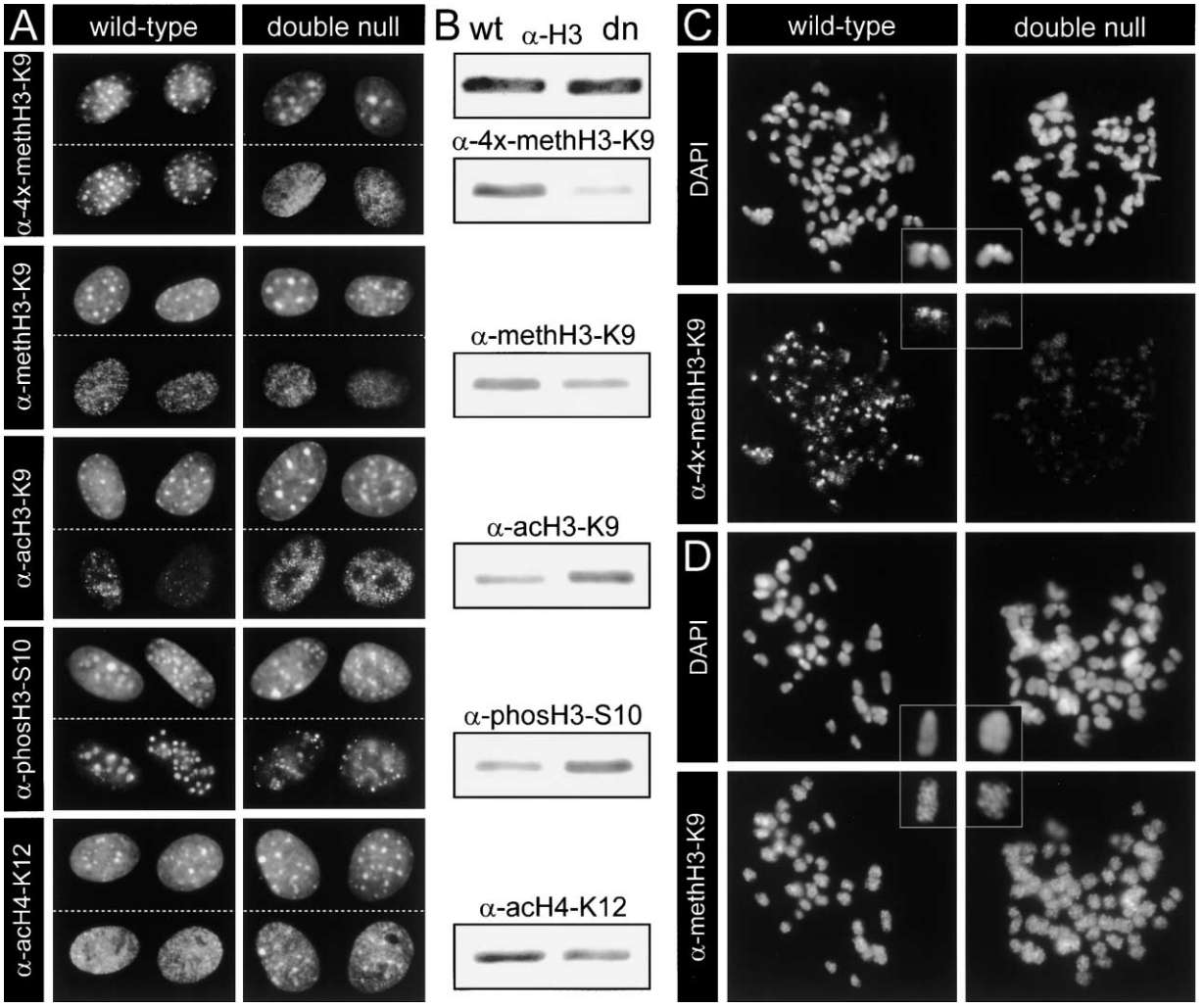

Figure 4. *Suv39h*-Dependent H3-K9 Methylation at Pericentric Heterochromatin

(A) Immunofluorescence of interphase chromatin in wild-type and *Suv39h* dn (double null) PMEFs with α-4x-methH3-K9, α-methH3-K9, α-acH3-K9, α-phosH3-S10, and α-acH4-K12 antibodies. DNA and heterochromatic foci were counterstained with DAPI and are displayed as the top images in each panel.

(B) Immunoblot analyses of precalibrated nuclear extracts from wt and *Suv39h* dn PMEF nuclear extracts with the above antibodies.

(C) DAPI and α-4x-methH3-K9 staining on mitotic chromosomes prepared from in vitro cultured wt and *Suv39h* dn bone marrow cells.

(D) DAPI and α-methH3-K9 staining on mitotic chromosomes prepared from wt and *Suv39h* dn PMEFs.

Insets in (C) and (D) show enlarged chromosomes.

ment at heterochromatic foci in interphase chromatin (Figure 4A). Moreover, the broad H3-K9 methylation visualized by the α-methH3-K9 antibodies was largely insensitive to the absence of Suv39h HMTase function. In agreement with these data, H3-K9 methylation did not appear as significantly reduced in nuclear extracts from *Suv39h* dn PMEFs as when analyzed with the α-4x-methH3-K9 antibodies (Figure 4B, top panels).

We next examined the in vivo abundance and nuclear distribution of histone tail modifications that could be regulated by H3-K9 methylation (e.g., H3-K9 acetylation and H3-S10 phosphorylation) (Rea et al., 2000), and which also have been shown to be important for pericentric heterochromatin organization, such as H3-S10 phosphorylation (Hendzel et al., 1997) and H4-K12 acetylation (Jeppesen et al., 1992; Turner, 2000). Comparative analyses of immunoblots containing precalibrated nuclear extracts (Figure 4B) and of immunofluorescence of interphase chromatin (Figure 4A) between wt and *Suv39h* dn PMEFs reveal that all of these histone tail modifications are altered in the absence of Suv39h HMTase function. For example, the speckled acH3-K9 staining is enhanced in *Suv39h* dn interphase chromatin, the G2-specific concentration of phosH3-S10 at heterochromatic foci (Hendzel et al., 1997) disperses into many small dots, and a fraction of acH4-K12 becomes enriched at heterochromatin. These data indicate that the histone tail modification pattern at pericentric heterochromatin is significantly perturbed in the absence of the Suv39h HMTases.

Hypogonadism and Complete Spermatogenic Failure in *Suv39h* dn Mice

In addition to their functions in somatic tissues, the expression pattern of the *Suv39h* HMTase genes suggests an important role during spermatogenesis (O'Car-

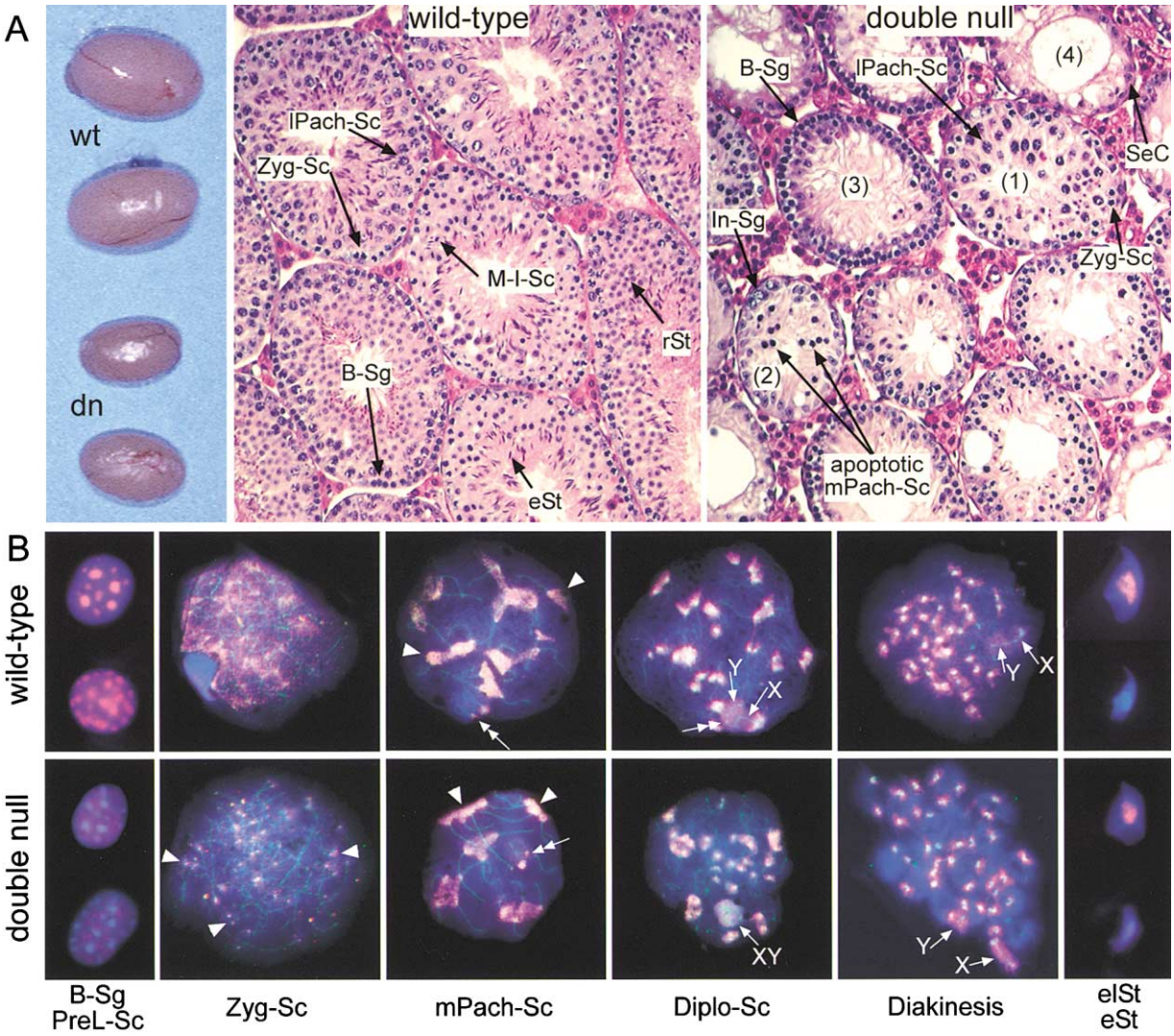

Figure 5. Spermatogenic Failure and H3-K9 Methylation in Germ Cells of *Suv39h* dn Mice

(A) Overall size and histology of wt and *Suv39h* dn testes at ~5 months of age. The *Suv39h* dn testis section reveals many seminiferous tubules that lack spermatocytes (Sc) and spermatids (St). Although a few seminiferous tubules (1) contain zygotene spermatocytes (Zyg-Sc), more advanced differentiation stages (2) display apoptotic spermatocytes (arrows) at pachytene (stage IV). At even later differentiation stages (3), pachytene spermatocytes are almost completely absent (stage V–VI). Some tubules (4) harbor only Sertoli cells (SeC). Abbreviations: Intermediate (In-Sg) and B-type spermatogonia (B-Sg); pre-leptotene (PreL-Sc), zygotene (Zyg-Sc), mid-pachytene (mPach-Sc), late-pachytene (lPach-Sc), diplotene (Diplo-Sc) and diakinesis/M-I (M-I-Sc) spermatocytes; round (rSt), elongating (elSt) and elongated (eSt) spermatids; Sertoli cells (SeC).

(B) Double-labeling immunofluorescence of wild-type (top panel) and *Suv39h* dn (bottom panel) germ cells with α-4x-methH3-K9 (pink) and α-Scp3 (green) antibodies. DNA was counterstained with DAPI (blue). In *Suv39h* dn germ cells, H3-K9 methylation is absent in proliferating spermatogonia (B-Sg) and in preleptotene spermatocytes (PreL-Sc). In zygotene spermatocytes (Zyg-Sc) only reduced 4x-methH3-K9 signals are detected at pericentric heterochromatin (arrowheads). At later stages, H3-K9 methylation appears in a wild-type staining (compare top and bottom panels), although *Suv39h* dn sex chromosomes (arrows) remain more intensely labeled at diplotene and diakinesis. The double arrow indicates the pseudo-autosomal region (PAR).

roll et al., 2000). Indeed, *Suv39h* dn males (n = 7) are infertile, do not contain mature sperm (data not shown) and their testis weights are 3- to 10-fold reduced as compared to that of wt males (Figure 5A). Histological sections demonstrate normally developed seminiferous tubules in wt testis. By contrast, spermatogenesis is severely impaired in *Suv39h* dn mice, with an apparent differentiation arrest at the transition between early to late spermatocytes, resulting in highly vacuolarized seminiferous tubules (Figure 5A).

We used FISH analyses with mouse major satellite DNA probes (Scherthan et al., 1996) and TUNEL assays to characterize the *Suv39h*-dependent spermatogenic defects further (data not shown). Mitotic proliferation of spermatogonia appeared normal, while the percentage of preleptotene spermatocytes was increased 3- to 10-fold. In addition, between mid- and late pachytene, most spermatocytes undergo apoptosis, resulting in stage V–VI tubules (see Figure 5A) that largely lack late pachytene spermatocytes and which do not contain haploid spermatids. These results suggest that the absence of *Suv39h* gene function induces delayed entry into meiotic

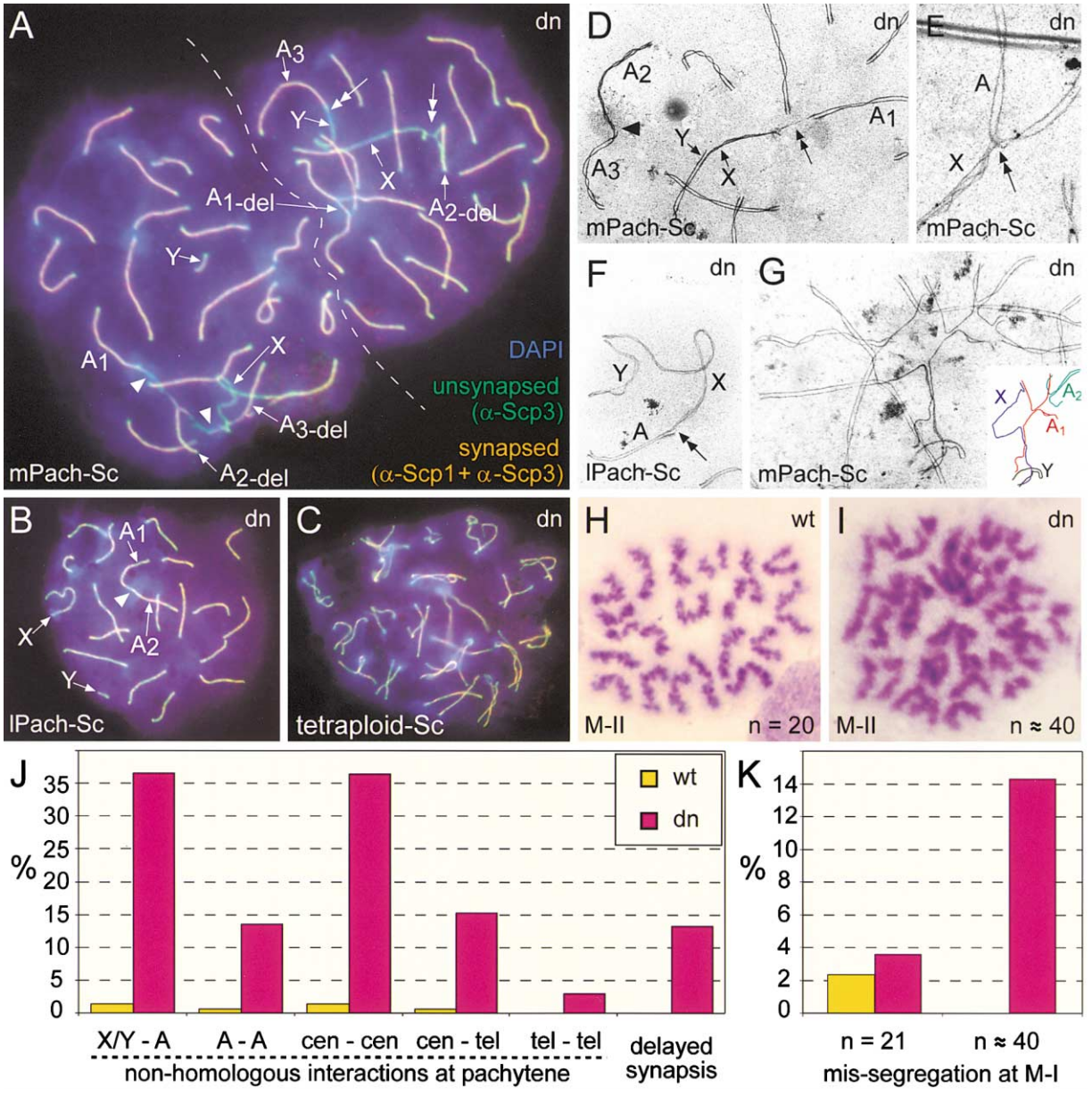

Figure 6. Illegitimate Associations and Delayed Synapsis of *Suv39h* dn Meiotic Chromosomes

(A–C) Double-labeling immunofluorescence of *Suv39h* dn pachytene spermatocytes with antibodies that are specific for the axial/lateral elements (α-Scp3 in green) and central elements (α-Scp1 in red) of the synaptonemal complex (SC). This colabeling reveals unsynapsed chromosomes in a green-like staining and synapsed chromosomes in an orange-red color. DNA was counterstained with DAPI (blue) which highlights pericentric heterochromatin in a more intense blue contrast. (A) Two mid-pachytene spermatocytes (mPach-Sc) showing multiple illegitimate associations (arrowheads) between nonhomologous autosomes (A) and between autosomes and sex chromomes (X, Y; double arrow). Several autosomes are also delayed in synapsis (A_{del}). (B) Late pachytene (lPach-Sc) spermatocyte containing two autosomes which are engaged in nonhomologous interaction through their pericentric regions (arrowhead). In addition, the sex chromosomes failed to pair. (C) Tetraploid spermatocyte resulting from complete missegregation of all chromosomes in the preceding mitotic division of a *Suv39h* dn spermatogonium.

(D–G) Transmission electron microscopy of *Suv39h* dn pachytene chromosomes, confirming that nonhomologous chromosome associations mainly occur through pericentric heterochromatin which is visualized by the more granular silver staining (arrowhead and double arrows). The chromosomes displayed in (G) show multiple engagements of partner exchange.

(H and I) Giemsa-stained metaphase II chromosomes of wt and *Suv39h* dn secondary spermatocytes illustrating complete missegregation in the preceeding meiosis I division of *Suv39h* dn cells.

(J) Histogram for the frequency of nonhomologous chromosome associations and delayed synapsis in wt (n = 80) and *Suv39h* dn (n = 90) pachytene spermatocytes.

(K) Histogram for the frequency of meiosis I missegregation of chromosome bivalents in wt (n = 40) and *Suv39h* dn (n = 30) secondary spermatocytes.

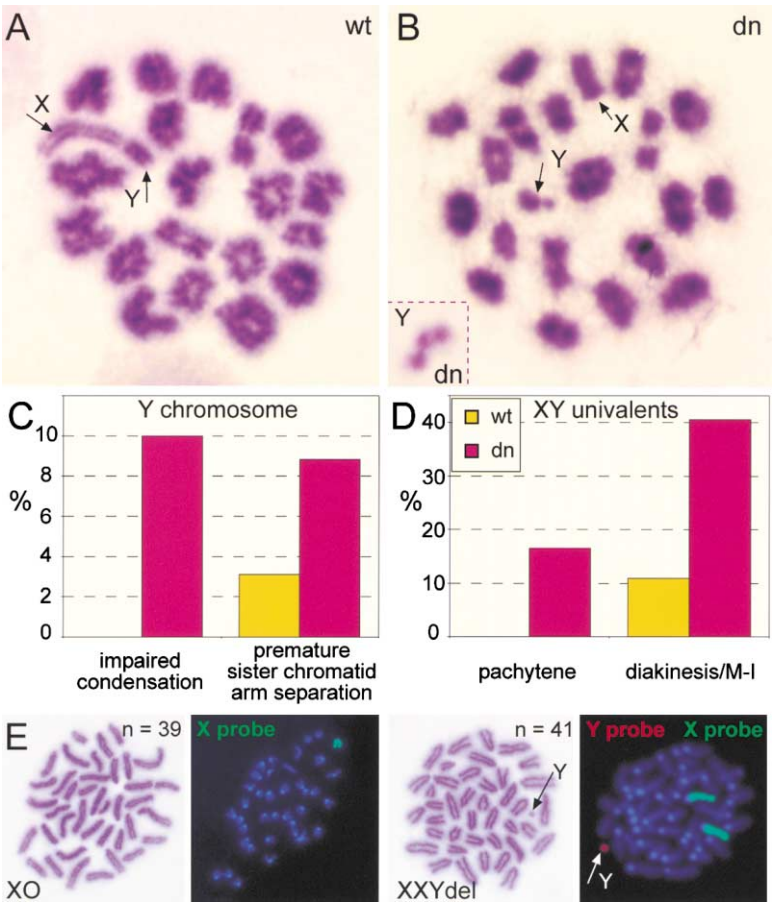

Figure 7. *Suv39h* Deficiency Induces Aberrant Sex Chromosome Segregation

Giemsa-stained diakinesis/metaphase-I chromosomes of wt (A) and *Suv39h* dn (B) primary spermatocytes illustrating univalency of the sex chromosomes. The inset in (B) shows a *Suv39h* dn Y chromosome with premature arm separation that was present in a different preparation. (C) Histogram for the frequency of diakinesis/M-I cells with abnormal condensation or premature sister chromatid separation of the Y chromosome (wt: n = 190; *Suv39h* dn: n = 170). (D) Histogram for the frequency of XY univalency at pachytene (wt: n = 80; *Suv39h* dn: n = 80) or diakinesis/M-I (wt: n = 190; *Suv39h* dn: n = 170). (E) FISH-analysis with sex chromosome painting probes indicating distorted X-Y recovery present at low frequency (e.g., ~6% for XO females) in offspring from *Suv39h* null1/het2 males.

prophase and triggers pronounced apoptosis of spermatocytes during the mid- to late pachytene stage.

H3-K9 Methylation at Meiotic Heterochromatin

To investigate whether the *Suv39h*-dependent spermatogenic failure could be correlated with a distinct impairment of meiotic heterochromatin, we analyzed testis spread preparations and cryosections (data not shown) with the α-4x-methH3-K9 antibodies. In wt preparations, these antibodies decorate heterochromatic foci in spermatogonia (B-Sg) and in preleptotene spermatocytes (preL-Sc) (Figure 5B, top panel). In early meiotic prophase (Zyg-Sc) and early pachytene, the methH3-K9 staining extended beyond heterochromatin into other chromatin regions. From mid-pachytene through diplotene and in diakinesis, the methH3-K9 staining was restricted to heterochromatic clusters which condense into one block of heterochromatin in elongating spermatids (Figure 5B, top panels). We did not detect 4x-methH3-K9 signals in elongated spermatids and mature spermatozoa, in which histones are replaced by protamines. The authenticity of this staining pattern had been confirmed in colocalization analyses with antibodies that recognize the synaptonemal complex (Lammers et al., 1995), HP1β (Turner et al., 2001), HP1γ (Minc et al., 2000), and phosH3-S10 (Cobb et al., 1999) (data not shown).

Impaired H3-K9 Methylation and Aneuploidies in *Suv39h* dn Germ Cells

In preparations from *Suv39h* dn testis spreads, 4x-methH3-K9 signals were absent in B-spermatogonia and pre-leptotene spermatocytes (Figure 5B, bottom panel). Further, we did not observe the broader chromatin staining that characterizes early spermatocytes (Zyg-Sc) at the onset of meiotic prophase. The impaired H3-K9 methylation was accompanied by a dispersed distribution of phosH3-S10 and partial delocalization of HP1γ in the majority of B-spermatogonia (data not shown), whereas HP1β was largely undetectable in both wt and *Suv39h* dn B-spermatogonia.

Surprisingly, from mid-pachytene onward, we observed wild-type staining for 4x-methH3-K9 at pericentric heterochromatin (Figure 5B, bottom panel). HP1β and HP1γ localization and phosH3-S10 signals at autosomes occurred normally in *Suv39h* dn late spermatocytes (data not shown). Thus, these results demonstrate that the Suv39h HMTases selectively regulate H3-K9 methylation in B-spermatogonia and at the very early stages of meiotic prophase. Similar to the analysis with PMEFs (see above), we observed an ~5-fold increased rate for missegregation of complete chromosome sets in *Suv39h* dn spermatogonia that results in tetraploid spermatocytes (see Figure 6C, below). In summary, our data define an early and stage-specific meiotic role for the Suv39h HMTases, and further suggest the existence of an additional H3-K9 HMTase(s) which can methylate

heterochromatin during meiotic prophase, diakinesis and in spermatids.

Nonhomologous Interactions and Delayed Synapsis in *Suv39h* dn Spermatocytes

The absence of pericentric H3-K9 methylation in spermatogonia and early spermatocytes is suggestive for a role of the Suv39h HMTases in defining a distinct higher-order chromatin structure that may be required for the initial alignments and clustering of meiotic chromosomes. We therefore analyzed chromosome synapsis by immunofluorescence of pachytene spreads with antibodies specific for the axial/lateral and central elements of the synaptonemal complex (SC) (Figures 6A and 6B). Intriguingly, in ~15% (n = 90) of *Suv39h* dn spermatocytes, we observed nonhomologous interactions between autosomes (Figure 6J). Nonhomologous interactions were even more frequent (~35%) between sex chromosomes and autosomes (X/Y-A). These illegitimate associations occurred predominantly between the acrocentric ends (cen-cen) of nonhomologous chromosomes, to a lesser extent between centromeres and telomeres (cen-tel) and only very rarely between telomeres (tel-tel) (Figure 6J). In addition, *Suv39h* dn spermatocytes contained unsynapsed sex chromosomes (see below) and autosomal bivalents that were delayed in synapsis. Delayed synapsis of autosomes (A-del) almost invariably correlated with nonhomologous associations (Figure 6A), suggesting that these processes are functionally related.

The illegitimate associations were further confirmed by transmission electron microscopy (Figures 6D–6G). These ultrastructural analyses revealed physical connections and bridge-like structures between the ends of nonhomologous chromosomes (double arrow in Figures 6D and 6F). We also observed the incidence of partner exchange (Figure 6G) and nonhomologous alignments (data not shown). None of these aberrant chromosomal interactions were detected in EM preparations from wt spermatocytes (data not shown).

Bivalent Missegregation at Meiosis I in *Suv39h* dn Spermatocytes

To investigate whether the absence of H3-K9 methylation in early prophase affects chromosome dynamics and segregation during the meiotic divisions, we next analyzed testis spread preparations for diakinesis/metaphase I (M-I) and metaphase II (M-II) cells. At diakinesis/M-I, most *Suv39h* dn spermatocytes revealed bivalents with wt-like morphology, indicating that chromosome condensation and chiasmata formation was unperturbed (but see Figures 7B–7D, below). However, at M-II, ~14% of secondary spermatocytes were tetraploid, indicating segregation failure of all bivalents during the first meiotic division (Figures 6I and 6K). Therefore, the *Suv39h*-induced defects at pericentric heterochromatin persist throughout the first meiotic division and do not appear to be "rescued" by the additional H3-K9 methylation that occurs during mid- to late meiotic prophase (see Figure 5B).

Suv39h Deficiency Interferes with Sex Chromosome Segregation

Spermatogenesis in male mammals is specialized by the presence of the heteromorphic sex chromosomes which form a unique chromatin region known as the sex vesicle or XY body (Solari, 1974). Moreover, the Y chromosome is the most heterochromatic chromosome in the mouse (Pardue and Gall, 1970). Homolog pairing and crossover between sex chromosomes is dependent upon the presence of a small, pseudo-autosomal region called PAR (Burgoyne, 1982). Absence of *Suv39h* gene function interferes with the chromatin organization and segregation of the sex chromosomes in several ways.

First, although 4x-methH3-K9 signals at the XY body (arrows in Figure 5B) were detected at comparable levels in wt and mutant pachytene spermatocytes, *Suv39h* dn sex chromosomes remain more heavily methylated in diplotene and diakinesis. Second, at diakinesis/M-I, the proximal region of the long arm of the Y chromosome appears hypo-condensed in 10% of *Suv39h* dn cells (Figures 7B and 7C). Moreover, the mutant Y chromosomes display premature separation of their arms (see inset in Figure 7B) or even complete separation of the two sister chromatids. Third, from pachytene onward, H3-K9 methylation is present at the PAR (double arrows in Figure 5B) in both wt and *Suv39h* dn sex chromosomes, and the PAR is also decorated with HP1β (data not shown) (Turner et al., 2001). Despite these similar staining patterns, the sex chromosomes failed to synapse in ~15% of *Suv39h* dn pachytene spermatocytes (Figures 6A and 6B). At diakinesis/M-I, the presence of XY univalents was elevated 4-fold as compared to wt cells (Figure 7D). Consistent with this increased univalency of the sex chromosomes, *Suv39h* null1/het2 males give rise to offspring that occasionally contain XO females (~6% of informative progeny; n = 167) and even one XXY male in which the distal part of the Y chromosomes was deleted (Figure 7E). Together, these data indicate a role for the Suv39h HMTases in coregulating the specialized chromatin structure of the sex chromosomes, in particular of the highly heterochromatic Y chromosome.

Discussion

Heterochromatin was first described more than 70 years ago (Heitz, 1928). Because of its stable appearance in the cell nucleus, it has been proposed to serve crucial functions for the inheritance of cell type identities and the fidelity of chromosome segregation during mitosis and meiosis. In this study, we establish the *Suv39h* HMTases as important chromatin regulators for mouse development and provide in vivo evidence that H3-K9 methylation at pericentric heterochromatin is required to protect genome stability in a mammalian organism.

Specificity and Redundancy of H3-K9 Methylation

Single gene disruptions for either *Suv39h1* or *Suv39h2* do not appear to affect viability and fertility of mutant mice. By contrast, combined disruption of both genes in *Suv39h* double null (dn) mice results in severly impaired development, with only one third of *Suv39h* dn mice surviving to adulthood. In addition, *Suv39h* dn mice are

growth retarded and infertile, both in males (see Figure 5A) and females (data not shown).

Using newly developed antibodies (α-4x-methH3-K9), we detect a specific dependence of H3-K9 methylation on Suv39h HMTase function at pericentric heterochromatin (see Figure 4). These data indicate that the Suv39h enzymes are the major HMTases for pericentric H3-K9 methylation, but do not significantly affect the broad H3-K9 methylation present in other chromsomal regions (see Figure 4). Thus, these α-4x-methH3-K9 antibodies suggest that not all H3-K9 methylation events cause the same alteration of the chromatin structure. This interpretation is supported by recent studies on the TSA-sensitivity of methylated heterochromatin (C. Maison et al., submitted). However, these observations do not exclude an additional role of the SUV39H1 HMTase in gene repression at euchromatic positions, which seems to be restricted to a rather local H3-K9 methylation pattern (Nielsen et al., 2001). We therefore propose that the dual functions of the Suv39h HMTases can be distinguished by the α-4x-methH3-K9 antibodies, which appear to be specific for a more regional transition in higher-order chromatin conformation.

The broad presence of H3-K9 methylation at nonpericentric regions in *Suv39h* dn chromatin indicates that additional HMTases modify the H3-K9 position. There are ~25 unique gene sequences in the mouse genome (F. Eisenhaber, personal communication) that contain the evolutionarily conserved SET domain and likely encode other HMTases (Jenuwein, 2001). At least two of these SET domain containing proteins, G9a (Tachibana et al., 2001) and ESET (A.K. and T.J., unpublished), can indeed also methylate H3 at lysine 9. Thus, the ~33% viability of *Suv39h* dn mice could, at least in part, be dependent on the compensating activity of these or other H3-K9 HMTases being expressed to varying degrees in the mixed genetic background in which the *Suv39h* dn mice were generated.

Genomic Instabilities and Tumorigenesis in *Suv39h*-Deficient Mice

The high lethality of *Suv39h* dn fetuses could be a consequence of altered control of epigenetic gene regulation and of perturbed chromosome segregation, with both mechanisms significantly impairing the proliferation and differentiation programs of the developing embryo. Although the recent link between the SUV39H1 HMTase and the tumor suppressor Rb (Nielsen et al., 2001) is likely to contribute to neoplastic transformation, the major phenotype observed in *Suv39h* dn mice is genomic instability in a variety of somatic cells (see Figures 2–3 and data not shown) and even in germ cells (see Figure 6). Moreover, *Suv39h*-deficient mice display a specifically increased risk for late-onset B cell lymphomas that also develop upon reduced *Suv39h1* gene dosage (see Table 1 and Figure 3B). The *Suv39h*-mediated genomic instability only affects a subpopulation of cells and does not appear to trigger pronounced apoptosis (see Figure 2B and data not shown).

Based on our results, we propose that Suv39h-dependent H3-K9 methylation is important for maintaining a stringent higher-order structure at pericentric heterochromatin, which is required to protect genomic stability. Absence of Suv39h HMTase function could result in a more "relaxed" heterochromatin organization prone to aberrant interactions and inducing chromosome missegregation by several mechanisms. First, *Suv39h* dn cells display more dispersed H3-S10 phosphorylation and perturbed enrichment of H4-K12 acetylation at heterochromatic foci (see Figure 4). Altered patterns of pericentric histone phosphorylation (Wei et al., 1999; Hsu et al., 2000) and acetylation (Ekwall et al., 1997; Taddei et al., 2001) mediate chromosome missegregation in a variety of model systems. Second, histone tail modifications can generate specific interaction affinities for chromatin-associated proteins (Jenuwein and Allis, 2001). Heterochromatic enrichment of HP1 is largely lost in *Suv39h* dn somatic cells (Lachner et al., 2001), whereas the localization of CENP epitopes appears unaltered (data not shown). These data argue against a direct role for Suv39h HMTases in centromere function, which would also be inconsistent with the relatively late embryonic lethality observed in the majority of *Suv39h* dn mice. Third, impaired recruitment of heterochromatin-associated proteins could also perturb possible interactions with cohesion complexes, in particular at pericentric heterochromatin (Waizenegger et al., 2000; R. Allshire, personal communication). Although a role for the Suv39h enzymes in cohesion at mammalian centromeres remains to be determined, the SUV39H1 HMTase dissociates from pericentric heterochromatin at the meta- to anaphase transition, in a signaling pathway that seems to be regulated by hyperphosphorylation of the SET domain (Aagaard et al., 2000).

Together, the possible mechanisms discussed above suggest that the *Suv39h* HMTases could act as tumor suppressor genes by maintaining H3-K9 methylation at pericentric heterochromatin. Downregulation and reduced heterochromatic accumulation of HP1α has recently been associated with an increased metastatic potential of tumor cells (Kirschmann et al., 2000).

Suv39h Deficiency Impairs Meiotic Chromosome Identity

Unlike in somatic cells, *Suv39h*-mediated defects in male meiosis induce pronounced apoptosis of stage IV spermatocytes during the transition from mid to late pachytene (see Figure 5A and data not shown). Activation of programmed cell death at this stage has also been observed in mouse mutants that are impaired in DNA damage control (Xu et al., 1996), meiotic recombination (Yoshida et al., 1998; de Vries et al., 1999; Baudat et al., 2000), and synaptonemal complex formation (Yuan et al., 2000). In *Suv39h* dn spermatocytes, pericentric H3-K9 methylation is specifically reduced at the preleptotene stage but, surprisingly, appears as wild-type staining during later meiotic stages (see Figure 5B, bottom panel). Thus, by analogy to the perturbed chromosome associations in somatic cells, we propose that impairment of pericentric H3-K9 methylation at the onset of meiosis may induce aberrant centromere clustering and random interactions that can not be resolved by the hypothetical activity of additional H3-K9 HMTases during pachytene. In *Suv39h*-deficient spermatocytes, meiotic chromosomes could be compromised in their ability to move more freely during the homolog search

or, alternatively, lack a stringent higher-order chromatin structure that appears to be required for partner recognition (Karpen et al., 1996; Dernburg et al.,1996; McKee et al., 2000). Our data characterize Suv39h-dependent H3-K9 methylation as one of the earliest requirements for successful meiosis. Because the failure to resolve nonhomologous interactions results in delayed synapsis or incomplete pairing (see Figure 6A), it triggers apoptosis by activating the pachytene checkpoint (de Vries et al., 1999), thereby protecting the male germline from accumulating aneuploidies.

Finally, *Suv39h* deficiency induces univalency of the sex chromosomes from pachytene to diakinesis that is further illustrated by distorted X-Y recovery in offspring from *Suv39h* null1/het2 males (see Figure 7). Intriguingly, HP1β (Turner et al., 2001) and the Suv39h2 HMTase (O'Carroll et al., 2000) localize to the specialized chromatin structure of the sex chromosomes in the XY body. Although XY body formation appears normal in early/mid pachytene of *Suv39h* dn spermatocytes, *Suv39h* deficiency prolongs H3-K9 methylation (see arrows in Figure 5B) and induces hypocondensation of the Y chromosome (see Figures 7B and 7C). These results implicate the Suv39h HMTase activities in the definition of the heterochromatic identity of the Y chromosome and suggest that *Suv39h*-mediated H3-K9 methylation may indirectly promote and/or stabilize homolog pairing of the heteromorphic sex chromosomes, probably by reinforcing the association potential of the pseudo-autosomal region (Turner et al., 2001).

Experimental Procedures

Generation and Genotyping of *Suv39h1*- and *Suv39h2*-Deficient Mice

Partial genomic clones of the *Suv39h1* locus (X chromosome) and of the *Suv39h2* locus (chromosome 2) (O'Carroll et al., 2000) were used to generate short and long arms of homology, in a strategy to produce in-frame fusion proteins of the first 40 amino acids of Suv39h1 or of the first 113 amino acids of Suv39h2 with β-galactosidase (LacZ) modified with a nuclear localization signal (nls) (see Figure 1A). The pGNA-derived targeting cassettes contained an RSV-*neomycin* (neo) gene for positive selection and two polyadenylation sites. The *diphtheria toxin A* (DTA) gene under the control of the MCI promoter (provided by T. Kallunki and M. Karin, San Diego, CA) was used to select against random integration and was inserted 3′ of the long arms of homology.

G418-resistant embryonic stem cell (R1 and E14.1) colonies were screened for homologous recombination by nested PCR using primers external to the short arms of *Suv39h1* (PCR1: 5′-ATGGGGGCAG GGTTTTCGGGTAGAC, PCR2: 5′-AAATGGTATTTGCAGGCCACTTC TTG) or of *Suv39h2* (PCR1: 5′-GAAAAGGTTGTTCTCCAGCTC, PCR2: 5′-GGATGGGATGGTGGAATGGTTTTTAT) and primers within the *lacZ* gene (lacZ-PCR1: 5′-AACCCGTCGGATTCTCCGTGGG AAC, lacZ-PCR2: 5′-CTCAGGAAGATCGCACTCCAGCC). Successful targeting was confirmed by Southern blot analysis of PvuII-digested ES cell DNA with an ~500 bp external *Suv39h1* intron probe, or of HindIII-digested ES cell DNA with an ~500 bp external *Suv39h2* exon/intron probe.

All mice described in this study were maintained on a mixed genetic background of 129/Sv and C57Bl/6J origin. Protein blot analysis of nuclear extracts from mouse testes with α-Suv39h1 and α-Suv39h2 antibodies was performed as described (O'Carroll et al., 2000).

Growth Curves and FACS Analyses of PMEFs

Mouse primary embryonic fibroblasts (PMEFs) were prepared from day E12.5 wild-type, *Suv39h1*−/−, *Suv39h2*−/−, and *Suv39h* dn fetuses as described (O'Carroll et al., 2000). To analyze their proliferative potential, PMEFs were seeded onto 10 cm^2 dishes. Over the next 30 passages, 3×10^5 cells were continually reseeded every third day onto a new 10 cm^2 dish (3T3 protocol), and their doubling rates determined. The DNA profiles of passage 3 and passage 8 PMEF cultures were obtained by FACS of ethanol-fixed and propidium-iodide stained cells, using chicken erythrocyte nuclei (Becton Dickinson) as an internal standard.

Immunohistochemistry of Tumor Sections

Spleen and lymph nodes from wt and tumor mice were fixed O/N in 2% p-FA, and 5 μm sections were processed for immunohistochemistry with α-4x-methH3-K9 antibodies (1:5,000 dilution in blocking solution) as described (Czvitkovich et al., 2001).

Bone Marrow Culture and FACS Analysis of B Cell Lymphoma Cells

Bone marrow cells from wt and *Suv39h* dn mice were cultivated for two weeks in StemPro-34 SFM medium (Life Technologies) supplemented with IL-3 (10 ng/ml), IL-6 (5 ng/ml), SCF (100 ng/ml), FLT 3 ligand (20 ng/ml), GM-CSF (1 ng/ml) (all from R&D Systems), 10 μM dexamethasone (Sigma) and IGF-1 (40 ng/ml) (Sigma). Cultures were grown at densities of ~3×10^6 cells per ml, and purified from differentiated and dead cells by Ficoll-Paque gradient centrifugation (Pharmacia).

Primary lymphoma cells were obtained from spleen and lymph nodes using a 70 μm Nylon Cell Strainer (Becton Dickinson), and cultivated in Iscove's modified Dulbecco's medium (IMDM) supplemented with 5% heat-inactivated fetal calf serum, 2 mM glutamine and 1% penicillin-streptomycin (all Gibco-BRL). Single cells suspensions were grown O/N in medium additionally containing 50 μM β-mercaptoethanol and 5% conditioned supernatant from rIL-7 producing J558L cells.

The identity of the tumor cells was determined by FACS analyses using antibodies (all from Pharmingen) that detect specific cell surface markers. All tumor cells were double positive for the B cell markers B220-low (RA3-6B2) and CD19 (1D3), but negative for the T cell markers CD3 (145-2C11), CD4 (RM4-5), CD8 (53-6.7), or for the granulocyte/ macrophage markers Gr-1 (RB6-8C5), Mac-1 (M1/70) and for a marker of the eythroid lineage, Ter-119. The majority of the B cell lymphoma cells were also double positive for CD43 (S7) and IgM (R6-60.2), while some clonal cultures displayed reactivity toward CD5 (53-7.3).

Chromosome Spreads and Karyotype Analyses

PMEF and tumor cell karyotypes were analyzed on colchicine-arrested and Giemsa-stained metaphase chromosome spreads as described (Czvitkovich et al., 2001).

Metaphase spreads of spermatogonia and spermatocytes were prepared from isolated seminiferous tubule fragments which had been hypotonically swollen with 1% sodium citrate for 10 min at RT and fixed O/N at 4°C with Carnoy's solution (75% methanol, 25% acetic acid). After incubation of seminiferous fragments in 60% acetic acid for 2 min, a single cell suspension was generated by repeated pipetting, transferred onto a pre-heated (60°C) glass slide, and cells were spread by mechanical shearing with a glass hockey stick.

The karyotype of XO females and XXY males was determined by fluorescent *in situ* hybridization using X and Y chromosome painting probes (Cambio) on metaphase spreads that had been prepared from peripheral lymphocytes after a three day stimulation with LPS and concavalin A.

Generation and Purification of α-4x-methH3-K9 Antibodies

A hexameric peptide, -TARK$(Me)_2$ST-, containing a dimethylated lysine (Bachem) was linked via C-terminal lysine residues to generate a "branched" peptide that consists of four -TARK$(Me)_2$ST- "fingers." The sequence of this branched peptide is [TARK$(Me)_2$ST]$_4$-K_2-K-cys. Crude antisera from two positive rabbits (#2233 and #2236) were batch-absorbed against a branched, but unmodified control peptide, followed by affinity purification against the dimethy-

lated branched antigen that had been crosslinked to a Poros™ column (Lachner et al., 2001). Bound antibodies were eluted with 100 mM glycine pH 2.5 and neutralized with 1/10 vol. of 2 M Hepes pH 7.9. The methyl-specificity of the antibodies was confirmed on slotblots presenting unmodified or K9-dimethylated histone H3 peptides. The affinity-purified α-4x-methH3-K9 antibodies (concentration ≈ 0.6 mg/ml) detect H3-K9 methylation in a wide variety of species (D. Schweizer, unpublished) and can be used at 1:1,000 dilution for protein blot analysis or at 1:1,000 to 1: 5,000 dilutions for indirect immunofluorescence.

Protein Blot Analysis for Histone Tail Modifications

Nuclear extracts were prepared from early passage wild-type and *Suv39h* dn PMEFs and precalibrated with α-H3 (Santa Cruz SC-8654) and α-HP1β (Serotec MAC353) antibodies. Approximately 10 μg of total nuclear extract was then separated by SDS-PAGE and analyzed with α-4x-methH3-K9, α-methH3-K9 (Upstate 07-212), α-acH3-K9 (Upsate 06-942), α-phosH3-S10 (Hendzel et al., 1997), and α-acH4-K12 (Taplik et al., 1998) antibodies.

Immunofluorescence of Interphase Chromatin and Metaphase Chromosomes

Immunofluorescence of interphase chromatin and metaphase chromosomes has been done as described (Aagaard et al., 2000; Melcher et al., 2000).

Testis Histology

Testes were dissected from adult mice, fixed in Bouins fluid (75% saturated picric acid, 5% glacial acetic acid, 9.3% formaldehyde) and stained with hematoxylin/eosine. FISH analyses with mouse major satellite DNA probes were done as described (Scherthan et al., 1996), and Tunel assays were performed using the DeadEnd apoptosis detection system (Promega). In addition, testis cryosections (O'Carroll et al., 2000) were also analyzed by immunofluorescence with α-Scp, α-HP1, α-phosH3-S10 and α-4x-meth H3-K9 antibodies (data not shown).

Immunofluorescence of Germ Cells and Meiotic Chromosome Spreads

Chromosome spreads of spermatogenic cells were prepared according to Peters et al. (1997) with some minor modifications. Double-labeling immunofluorescence of germ cell preparations was performed by sequential incubation with rabbit polyclonal α-4x-methH3-K9 antibodies and with goat α-rabbit Alexa568-conjugated secondary antibodies. After a brief fixation in 1% p-FA, samples were incubated with rabbit polyclonal α-Scp3 antibodies (Lammers et al., 1995) that were visualized with goat α-rabbit Alexa488-conjugated secondary antibodies. In addition, costainings were also done with α-Scp3 and α-Scp1 (Scherthan et al., 1996), and α-Scp3 and HP1β (Serotec MAC353), and α-Scp3 and α-phosH3-S10 (Hendzel et al., 1997) antibodies (data not shown).

EM Analysis

Preparation and silver staining of SC complexes from spread germ cells was performed according to Peters et al. (1997). Slides were incubated with 50% $AgNO_3$ under a nylon mesh for 1 hr at 60°C and then for another 1 hr at 50°C. After four washes in double-distilled water and thorough air-drying, slides were coated with a film prepared from a 1% (w/v) Falcon plastic solution in chloroform, and overlaid with copper grids. Visually preselected nuclei were released from the glass slide to the film-coated copper grids by careful addition of 2.5% hydrofluoric acid. Grids were analyzed on a Jeol 1200 EKII transmission electron microscope.

Acknowledgments

We are particularly grateful to Dieter Schweizer (Institute of Botany, Vienna University) for advice and help during the initial analysis of the spermatogenic defects in *Suv39h*-deficient mice. We thank Frank Eisenhaber and Alexander Schleiffer for database searches on SET domain sequences, Lukas Kenner for advice on the characterization of tumor sections, Martin Jerratsch (University of Kaiserslautern) for technical assistance, Christa Heyting (Wageningen University, The Netherlands) for α-Scp antibodies, Christian Seiser (Vienna Biocenter) for α-acH4-K12 antibodies, and Robin Allshire (MRC, Edinburgh) for communicating unpublished results. We also thank Peter de Boer (Wageningen University, the Netherlands), Dieter Schweizer and an anonymous reviewer for helpful comments on the manuscript. This work was supported by the IMP through Boehringer Ingelheim and by grants from by the Austrian Research Promotion Fund and the Vienna Economy Promotion Fund to T.J., and by the Deutsche Forschungsgemeinschaft (grant number DFG #350/8-3) to H.S.

Received May 21, 2001; revised September 27, 2001.

References

Aagaard, L., Schmid, M., Warburton, P., and Jenuwein, T. (2000). Mitotic phosphorylation of SUV39H1, a novel component of active centromeres, coincides with transient accumulation at mammalian centromeres. J. Cell Sci. *113*, 817–829.

Allshire, R.C., Nimmo, E.R., Ekwall, K., Javerzat, J.P., and Cranston, G. (1995). Mutations derepressing silent centromeric domains in fission yeast disrupt chromosome segregation. Genes Dev. *9*, 218–233.

Bannister, A.J., Zegerman, P., Partridge, J.F., Miska, E.A., Thomas, J.O., Allshire, R.C., and Kouzarides, T. (2001). Selective recognition of methylated lysine 9 on histone H3 by the HP1 chromo domain. Nature *410*, 120–124.

Baudat, F., Manova, K., Yuen, J.P., Jasin, M., and Keeney, S. (2000). Chromosome synapsis defects and sexually dimorphic meiotic progression in mice lacking *spo11*. Mol. Cell *6*, 989–998.

Bird, A., and Wolffe, A.P. (1999). Methylation-induced repression—belts, braces and chromatin. Cell *99*, 451–454.

Burgoyne, P.S. (1982). Genetic homology and crossing over in the X and Y chromosomes of mammals. Hum. Genet. *61*, 85–90.

Cobb, J., Miyaike, M., Kikuchi, A., and Handel, M.A. (1999). Meiotic events at the centromeric heterochromatin: histone H3 phosphorylation, topoisomerase II alpha localization and chromosome condensation. Chromosoma *108*, 412–425.

Csink, A.K., and Henikoff, S. (1998). Something from nothing: the evolution and utility of satellite repeats. Trends Genet. *14*, 200–204.

Czvitkovich, S., Sauer, S., Peters, A.H.F.M., Deiner, E., Wolf, A., Laible, G., Opravil, S., Beug, H., and Jenuwein, T. (2001). Overexpression of the SUV39H1 histone methyltransferase induces altered proliferation and differentiation in transgenic mice. Mech. Dev. *107*, 141–153.

Dernburg, A.F., Sedat, J.W., and Hawley, R.S. (1996). Direct evidence of a role for heterochromatin in meiotic chromosome segregation. Cell *86*, 135–146.

de Vries, S.S., Baart, E.B., Dekker, M., Siezen, A., de Rooij, D.G., de Boer, P., and te Riele, H. (1999). Mouse MutS-like protein Msh5 is required for proper chromosome synapsis in male and female meiosis. Genes Dev. *13*, 523–531.

Eissenberg, J.C., Morris, G.D., Reuter, G., and Hartnett, T. (1992). The heterochromatin-associated protein HP-1 is an essential protein in *Drosophila* with dosage-dependent effects on position-effect variegation. Genetics *131*, 345–352.

Ekwall, K., Nimmo, E.R., Javerzat, J.P., Borgstrom, B., Egel, R., Cranston, G., and Allshire, R. (1996). Mutations in the fission yeast silencing factors clr4+ and rik1+ disrupt the localisation of the chromo domain protein Swi6p and impair centromere function. J. Cell Sci. *109*, 2637–2648.

Ekwall, K., Olsson, T., Turner, B.M., Cranston, G., and Allshire, R.C. (1997). Transient inhibition of histone deacetylation alters the structural and functional imprint at fission yeast centromeres. Cell *91*, 1021–1032.

Fanti, L., Giovinazzo, G., Berlocco, M., and Pimpinelli, S. (1998). The heterochromatin protein 1 prevents telomere fusions in *Drosophila*. Mol. Cell *2*, 527–538.

Firestein, R., Cui, X., Huie, P., and Cleary, M.L. (2000). SET domain-

dependent regulation of transcriptional silencing and growth control by SUV39H1, a mammalian ortholog of *Drosophila* Su(var)3-9. Mol. Cell. Biol. *20*, 4900–4909.

Foon, K.A., and Gale, R.P. (1995). Chronic Lymphoid Leukemias. In Blood: Principles and Practice of Hematology, R.I. Handin, T.P. Stossel, and S.E. Lux, eds. (Philadelphia: J.B. Lippincott Company), pp. 783–811.

Heitz, E. (1928). Das Heterochromatin der Moose. Jhrb. Wiss. Botanik *69*, 762–818.

Hendzel, M.J., Wei, Y., Mancini, M.A., Van Hooser, A., Ranalli, T., Brinkley, B.R., Bazett-Jones, D.P., and Allis, C.D. (1997). Mitosis-specific phosphorylation of histone H3 initiates primarily within pericentromeric heterochromatin during G2 and spreads in an ordered fashion coincident with mitotic chromosome condensation. Chromosoma *106*, 348–360.

Henikoff, S., Ahmad, K., and Malik, H.S. (2001). The centromere paradox: stable inheritance with rapidly evolving DNA. Science *293*, 1098–1102.

Hsu, J.Y., Sun, Z.W., Li, X., Reuben, M., Tatchell, K., Bishop, D.K., Grushcow, J.M., Brame, C.J., Caldwell, J.A., Hunt, D.F., et al. (2000). Mitotic phosphorylation of histone H3 is governed by Ipl1/aurora kinase and Glc7/PP1 phosphatase in budding yeast and nematodes. Cell *102*, 279–291.

Ivanova, A.V., Bonaduce, M.J., Ivanov, S.V., and Klar, A.J. (1998). The chromo and SET domains of the Clr4 protein are essential for silencing in fission yeast. Nat. Genet. *19*, 192–195.

Jenuwein, T. (2001). Re-SET-ting heterochromatin by histone methyltransferases. Trends Cell Biol. *11*, 266–273.

Jenuwein, T., and Allis, C.D. (2001). Translating the histone code. Science *293*, 1074–1080.

Jeppesen, P., Mitchell, A., Turner, B.M., and Perry, P. (1992). Antibodies to defined histone epitopes reveal variations in chromatin conformation and underacetylation of centromeric heterochromatin in human metaphase chromosomes. Chromosoma *101*, 322–332.

Karpen, G.H., and Allshire, R.C. (1997). The case for epigenetic effects on centromere identity and function. Trends Genet. *13*, 489–496.

Karpen, G.H., Le, M.H., and Le, H. (1996). Centric heterochromatin and the efficiency of achiasmate disjunction in *Drosophila* female meiosis. Science *273*, 118–122.

Kellum, R., and Alberts, B.M. (1995). Heterochromatin protein 1 is required for correct chromosome segregation in *Drosophila* embryos. J. Cell Sci. *108*, 1419–1431.

Kingston, R.E., and Narlikar, G.J. (1999). ATP-dependent remodeling and acetylation as regulators of chromatin fluidity. Genes Dev. *13*, 2339–2352.

Kirschmann, D.A., Lininger, R.A., Gardner, L.M., Seftor, E.A., Odero, V.A., Ainsztein, A.M., Earnshaw, W.C., Wallrath, L., and Hendrix, M.J. (2000). Down-regulation of HP1Hs alpha expression is associated with the metastatic phenotype in breast cancer. Cancer Res. *60*, 3359–3363.

Lachner, M., O'Carroll, D., Rea, S., Mechtler, K., and Jenuwein, T. (2001). Methylation of histone H3 lysine 9 creates a binding site for HP1 proteins. Nature *410*, 116–120.

Lammers, J.H., van Aalderen, M., Peters, A.H.F.M., van Pelt, A.A., de Rooij, D.G., de Boer, P., Offenberg, H.H., Dietrich, A.J., and Heyting, C. (1995). A change in the phosphorylation pattern of the 30,000-33,000 Mr synaptonemal complex proteins of the rat between early and mid-pachytene. Chromosoma *104*, 154–163.

Lyko, F. (2001). DNA methylation learns to fly. Trends Genet. *17*, 169–172.

McKee, B.D., Hong, C.S., and Das, S. (2000). On the roles of heterochromatin and euchromatin in meiosis in *Drosophila*: mapping chromosomal pairing sites and testing candidate mutations for effects on X-Y nondisjunction and meiotic drive in male meiosis. Genetica *109*, 77–93.

Melcher, M., Schmid, M., Aagaard, L., Selenko, P., Laible, G., and Jenuwein, T. (2000). Structure-function analysis of SUV39H1 reveals a dominant role in heterochromatin organization, chromosome segregation, and mitotic progression. Mol. Cell. Biol. *20*, 3728–3741.

Minc, E., Courvalin, J.C., and Buendia, B. (2000). HP1 gamma associates with euchromatin and heterochromatin in mammalian nuclei and chromosomes. Cytogenet. Cell Genet. *90*, 279–284.

Murphy, T.D., and Karpen, G. (1998). Centromeres take flight: alpha satellite and the quest for the human centromere. Cell *93*, 317–320.

Nakayama, J., Rice, J.C., Strahl, B.D., Allis, C.D., and Grewal, S.I.S. (2001). Role of histone H3 lysine 9 methylation in epigenetic control of heterochromatin assembly. Science *292*, 110–113.

Nielsen, S.J., Schneider, R., Bauer, U.-M., Bannister, A.J., Morrison, A., O'Carroll, D., Firestein, R., Cleary, M., Jenuwein, T., Herrera, R.E., and Kouzarides, T. (2001). Rb targets histone H3 methylation and HP1 to promoters. Nature *412*, 561–565.

O'Carroll, D., Scherthan, H., Peters, A.H.F.M., Opravil, S., Haynes, A.R., Laible, G., Rea, S., Schmid, M., Lebersorger, A., Jerratsch, M., et al. (2000). Isolation and characterization of *Suv39h2*, a second histone H3 methyltransferase gene that displays testis-specific expression. Mol. Cell. Biol. *20*, 9423–9433.

Pardue, M.L., and Gall, J.G. (1970). Chromosomal localization of mouse satellite DNA. Science *168*, 1356–1358.

Peters, A.H.F.M., Plug, A.W., van Vugt, M.J., and de Boer, P. (1997). A drying-down technique for the spreading of mammalian meiocytes from the male and female germline. Chromosome Res. *5*, 66–68.

Rea, S., Eisenhaber, F., O'Carroll, D., Strahl, B.D., Sun, Z.W., Schmid, M., Opravil, S., Mechtler, K., Ponting, C.P., Allis, C.D., and Jenuwein, T. (2000). Regulation of chromatin structure by site-specific histone H3 methyltransferases. Nature *406*, 593–599.

Scherthan, H., Weich, S., Schwegler, H., Heyting, C., Harle, M., and Cremer, T. (1996). Centromere and telomere movements during early meiotic prophase of mouse and man are associated with the onset of chromosome pairing. J. Cell Biol. *134*, 1109–1125.

Solari, A.J. (1974). The behavior of the XY pair in mammals. Int. Rev. Cytol. *38*, 273–317.

Strahl, B.D., and Allis, C.D. (2000). The language of covalent histone modifications. Nature *403*, 41–45.

Tachibana, M., Sugimoto, K., Fukushima, T., and Shinkai, Y. (2001). SET-domain containing protein, G9a, is a novel lysine-preferring mammalian histone methylthansferase with hyperactivity and specific selectivity to lysines 9 and 27 of histone H3. J. Biol. Chem. *276*, 25309–25317.

Taddei, A., Maison, C., Roche, D., and Almouzni, G. (2001). Reversible disruption of pericentric heterochromatin and centromere function by inhibiting deacetylases. Nat. Cell Biol. *3*, 114–120.

Taplik, J., Kurtev, V., Lagger, G., and Seiser, C. (1998). Histone H4 acetylation during interleukin-2 stimulation of mouse T-cells. FEBS Lett. *436*, 349–352.

Thon, G., Cohen, A., and Klar, A.J.S. (1994). Three additional linkage groups that repress transcription and meiotic recombinaiton in the mating-type region of *Schizosaccharomyces pombe*. Genetics *138*, 29–38.

Tschiersch, B., Hofmann, A., Krauss, V., Dorn, R., Korge, G., and Reuter, G. (1994). The protein encoded by the *Drosophila* position-effect variegation suppressor gene *Su(var)3-9* combines domains of antagonistic regulators of homeotic gene complexes. EMBO J. *13*, 3822–3831.

Turner, B.M. (2000). Histone acetylation and an epigenetic code. Bioassays *22*, 836–845.

Turner, J.M., Burgoyne, P.S., and Singh, P.B. (2001). M31 and macroH2A1.2 colocalize at the pseudoautosomal region during mouse meiosis. J. Cell Sci., in press.

Waizenegger, I.C., Hauf, S., Meinke, A., and Peters, J.M. (2000). Two distinct pathways remove mammalian cohesin from chromosome arms in prophase and from centromeres in anaphase. Cell *103*, 399–410.

Wei, Y., Yu, L., Bowen, J., Gorovsky, M.A., and Allis, C.D. (1999). Phosphorylation of histone H3 is required for proper chromosome condensation and segregation. Cell *97*, 99–109.

Xu, Y., Ashley, T., Brainerd, E.E., Bronson, R.T., Meyn, M.S., and Baltimore, D. (1996). Targeted disruption of ATM leads to growth retardation, chromosomal fragmentation during meiosis, immune defects, and thymic lymphoma. Genes Dev. *10*, 2411–2422.

Yoshida, K., Kandoh, G., Matsuda, Y., Habu, T., Nishimune, Y., and Morita, T. (1998). The mouse RecA-like gene *Dmc1* is required for homologous chromosome synapsis during meiosis. Mol. Cell *1*, 707–718.

Yuan, L., Liu, J.G., Zhao, J., Brundell, E., Daneholt, B., and Hoog, C. (2000). The murine Scp3 gene is required for synaptonemal complex assembly, chromosome synapsis, and male fertility. Mol. Cell *5*, 73–83.